RESEARCH

Measurements in a Turbulent Channel Flow by Means of an LDV Profile Sensor

Saskia Pasch[1] · Robin Leister[1] · Davide Gatti[1] · Ramis Örlü[2] ·
Bettina Frohnapfel[1] · Jochen Kriegseis[1]

© The Author(s) 2023

Abstract

Spatially and temporally resolved velocity measurements in wall-bounded turbulent flows remain a challenge. Contrary to classical laser Doppler velocimetry (LDV) measurements, the laser Doppler velocity profile sensor (LDV-PS) allows the combined measurement of tracer particle position and velocity, which makes it a promising tool. To assess its feasibility a commercial LDV-PS is employed in a turbulent channel flow at $Re_\tau = 350$. Additionally, the measurement and signal-processing accuracies of velocity and location are evaluated for various tracer-object sizes and velocities. On this basis, the turbulent channel flow measurements are evaluated and compared to reference data from direct numerical simulations. Thus, potentials of the LDV-PS are investigated for different regions of the flow and various data processing routines as well as the experimental practice are discussed from an application perspective.

1 Introduction

Detailed near-wall measurements of turbulent flows are fundamental for the understanding and assessment of different flow control techniques, whether they be aimed to reliably quantify any drag reduction effect or investigate the underlying mechanisms. The present study considers a commercial laser Doppler velocity profile sensor (LDV-PS) (ILA R&D GmbH 2023), which is employed in a turbulent channel flow. The use of such a sensor is motivated by active flow control strategies e.g. based on plasma actuators, which impose stringent requirements to experimental setup and suitable diagnostic tools, partially

---

R. Örlü: Mercator Fellow at Karlsruhe Institute of Technology.

✉ Saskia Pasch
  saskia.pasch@kit.edu

1   Institute of Fluids Mechanics (ISTM), Karlsruhe Institute of Technology (KIT), Kaiserstraße 10, 76131 Karlsruhe, Germany

2   Linné FLOW Centre, Engineering Mechanics, KTH Royal Institute of Technology, 100 44 Stockholm, Sweden

ⓐ Springer

excluding conventional measurement techniques such as thermal anemometry. The major objective of the present investigation, therefore, is an evaluation of the LDV-PS as a non-intrusive measurement technique for velocity-profile diagnostics of the considered canonical channel flow. A complementary parametric study is conducted with the aim of characterising the measurement accuracy of the applied LDV-PS measurement system, on basis of which the channel flow measurements are interpreted.

1.1 Motivation

For the evaluation of flow control efforts in wall-bounded turbulent flows, the turbulent channel flow serves as a widely used, well documented reference flow, allowing a direct comparison of actuated and non-actuated flow cases as well as experimental and numerical data. Therefore, in the present work, streamwise velocity measurements in a fully developed turbulent channel flow are considered to investigate the feasibility of the LDV-PS measurement system. Near-wall measurements are of special interest for turbulent drag reduction. In particular, the wall shear stress and thus the local skin friction drag can be directly deduced from the velocity gradient at the wall if this quantity can be resolved experimentally. Capturing near-wall turbulence in our channel flow facility demands a spatial resolution in the sub-millimeter range, which places high requirements on the measurement technology. Therefore, in the next section a brief overview of the most established measurement techniques in near-wall turbulent flows is given. On this basis, the possibilities offered by LDV-PS as an additional flow diagnostic means are assessed.

1.2 Turbulent Flow Measurements Near Solid Walls

Hot wire anemometry (HWA) is an intrusive measurement technique with which flow velocities can be derived from the heat transfer of a wire probe exposed to a flow (Bruun 1995). The measurement quantities are averaged over the probe length, which accordingly limits the achievable spatial resolution. As the wire length has to be around 200 times larger than its diameter to reduce the influence of heat conduction at the prongs (Ligrani and Bradshaw 1987), the smallest scales of turbulence may not be resolved by this measurement technique depending on the length scales of the flow under investigation. To overcome this limitation, microelectromechanical system (MEMS) manufacturing methods have been used to build miniature probes of which the most recent and promising are so-called nanoscale thermal anemometry probes (NSTAP) (Fan et al. 2015), which have reduced the sensing element compared to classical HWA probes by an order of magnitude. Nevertheless, thermal anemometry probes in general suffer from well-known wall-interference effects that can cause measurement errors, which limits the applicability of hot wire measurements especially in the viscous sublayer (Alfredsson et al. 2011). Especially in complex flows as those manipulated by active flow control techniques, HWA is sensitive to variations in ambient temperature e.g. in the near vicinity of dielectric barrier discharge plasma actuators. In addition, in the context of plasma actuators such measurements are nearly impossible due to the contamination of the hot-wire signal from electromagnetic interference as well as the danger of damaging the HWA circuit due an electrical arcing between the exposed electrode and the hot-wire probe (Kotsonis 2015; Benard and Moreau 2014).

Particle image velocimetry (PIV) is an optical, non-intrusive measurement technique based on the evaluation of the displacement of particle images, which were acquired

at two different time instances. The resolution is determined by the choice of the size and overlap of so-called interrogation areas within which the mean particle velocity is evaluated (Raffel et al. 2018). With a suitable setup and processing routine, micrometer spatial resolution can be achieved (Raffel et al. 2018; Cierpka et al. 2013; Meinhart et al. 2000; Fuchs et al. 2023).

Due to the challenges of obtaining accurate PIV results in the immediate vicinity of walls related to sparse and inhomogeneous seeding, Particle Tracking Velocimetry (PTV) is often used as a complement to standard PIV setups (Kähler et al. 2012). Such an approach has e.g. been followed by Cierpka et al. (2013), who performed measurements of the velocity profile in a turbulent boundary layer by combining PIV measurements in shifted fields of view with different magnifications and PTV measurements to capture the flow speed in different orders of magnitude simultaneously. PIV-specific perspective errors may occur due to the finite width of the laser light sheet and were shown to be compensated in a parallax correction procedure.

Recently volumetric defocusing μPTV was successfully applied to resolve the viscous sublayer of a turbulent boundary layer through a single optical access for the wall shear stress determination (Fuchs et al. 2023). Again, the method was suggested as a complement for large-scale measurements captured with a different setup. The seeding of the near-wall region, which is the basis for most optical measurement applications, was reported to be challenging.

These two PTV-based measurement setups allow a local evaluation of the wall shear stress and are likely suitable even under the challenging conditions of a plasma-forced flow. However, a parallax position correction might be restricted due to a non-reflective surface of the actuator. Generally, it has been observed that particle-based measurement techniques can be affected by electromagnetic fields as those occurring around plasma actuators when particles receive electrical charge. However, these effects are expected to exert minor influence on measurement results (Kotsonis 2015; Benard and Moreau 2014).

Laser Doppler velocimetry (LDV) is another laser- and particle-based measurement technique. For general LDV measurements the spatial resolution is limited to the size of the measurement volume in the order of magnitude of several hundreds of μm (Tropea et al. 2007), since the positions at which tracer particles cross the measurement volume cannot be distinguished. In consequence, the Doppler-burst signals of all registered particles within the measurement volume are converted into a single velocity value for the entire measurement volume – independent from the variety of individual particle trajectories and velocities. Furthermore, various bias errors might occur with this measurement technique, as elaborated in the treatise of Albrecht et al. (2013). One of these is caused by an uneven distribution of particles passing the measurement volume at different velocities, as a higher number of particle occurrences may be expected in regions of higher mean velocity. Another possible bias error is related to the elliptical shape of the measurement volume and the velocity gradient within it, as the measurement volume is wider at its center such that more particles might be detected in this region.

Other techniques related to time-resolved measurements in the viscous sublayer have recently been reviewed in Örlü and Vinuesa (2020) highlighting that state-of-the-art techniques are faced with various challenges besides temporal and spatial resolution, or limitations in their dynamic range. The current work therefore also comprises a contribution to explore and assess the potential of LDV-PS for measurements in the viscous sublayer.

1.3 Related Work Using the LDV-PS

The LDV-PS measurement technique, in contrast to a standard LDV described above, can spatially resolve the velocity profile within the measurement volume (Czarske 2001; Czarske et al. 2002). The measurement technique was further improved and developed (Büttner and Czarske 2003, 2006; Bayer et al. 2008), and has been shown to be capable of measuring turbulent channel flow mean velocity profiles as well as fluctuations in the main flow direction (Shirai et al. 2006). As additional fields of application, an LDV-PS was used to measure the acoustic particle velocity (Haufe et al. 2014), the flow in a fuel cell stack (Bürkle et al. 2020) and a microfluidic air flow (Bürkle et al. 2022a). Recently, Bürkle et al. (2022b) reported the flow characterization of a the gas flow in a model experiment for crystal growth by means of combined PIV and LDV-PS measurements for large and small scale investigations.

In the present work, a recently introduced commercial ILA R&D LDV-PS system with an integrated 5 MHz Bragg shift is employed, which was shown to allow measurements in a laminar Couette-like oil flow in a clutch test rig (Leister et al. 2022). The commercial measurement system has furthermore been successfully applied to measure the turbulent flow in the wake of a droplet with a spatial resolution of 10 µm (Burgmann et al. 2021) and the flow topologies appearing in rotary pumps used for blood (Strauch et al. 2022). The two above-mentioned studies, therefore, present the LDV-PS as a promising diagnostics tool for non-intrusive measurements in turbulent flows.

2 Experimental Procedure

The experimental procedure of LDV-PS measurements is elaborated in the present section, which first addresses the LDV-PS working principle in Sect. 2.1. Subsequently, two sets of conducted experiments are introduced. Particularly, the setup of the measurements in the turbulent channel flow is introduced in Sect. 2.2 to study the LDV-PS capabilities for the given flow scenario. An additional characterization study is introduced in Sect. 2.3, which – in continuation of earlier characterization efforts by Pasch et al. (2022) – particularly aims at a decomposition of different sources of uncertainty during experimentation with the LDV-PS.

2.1 LDV-PS Working Principle

The LDV-PS builds upon the laser Doppler Velocimetry (LDV) measurement concept: two laser-beam pairs $i = 1, 2$ with different wavelengths λ_i cross building overlapping interference fringe systems in the same plane. In contrast to a general LDV arrangement, the intersection points of the pairs are shifted from their respective beam-waist positions to the converging and diverging parts of the beams to purposely span two overlapping counter-oriented fan-shaped fringe patterns (Czarske 2001). Consequently, the fringe distances d_i with $i = 1, 2$ of the resulting interference patterns are a function of the y-position as illustrated in Fig. 1 for one beam pair. Since the registered Doppler-burst signals of a single particle – while simultaneously crossing both fringe patterns accordingly – rely on the

Fig. 1 Convergent fringe pattern of one laser-beam pair with intersection point shifted from the beam waists
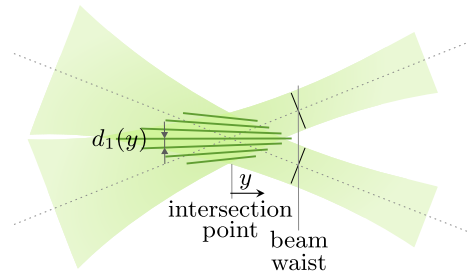
location within the ellipsoid, the y-position can be determined with the quotient q of the received scattered light frequencies f_i of both fringe systems, i.e.

$$q(y) = \frac{f_2(y,u)}{f_1(y,u)} = \frac{u/d_2(y)}{u/d_1(y)} = \frac{d_1(y)}{d_2(y)}, \tag{1}$$

as elaborated by Czarske et al. (2002). The fringe distances $d_i(y)$ of either beam pair and the resulting quotient function $q(y)$ according to (1) are shown in Fig. 2 as green solid and gray dashed lines, respectively. Furthermore, a linearized version of the frequency quotient, i.e. q^*, is added to the diagram as black solid line, which serves as calibration to assign a y-position value to the measured frequencies in pre-calibrated set-ups as used in the present study. The uncertainty of the y-position-estimation procedure (1) has been derived theoretically in terms of standard deviations for the y-position

$$\sigma_y \approx \sqrt{2} \left\| \frac{\partial y}{\partial q} \right\| \frac{\sigma_f}{f} \tag{2}$$

and corresponding velocity

$$\frac{\sigma_u}{u} \approx \sqrt{\frac{3}{2}} \frac{\sigma_f}{f} \tag{3}$$

by Czarske et al. (2002) assuming similar frequency levels and standard deviations in both fringe systems. It is consequently concluded, that the LDV-PS measurement accuracy depends on the accuracy at which the Doppler frequencies f_1 and f_2 are captured, the slope $\partial q/\partial y$ of the calibration curve and the accuracy of the calibration curve.

The commercial LDV-PS used in this work combines all laser light sources, optical components and the photo multiplier detecting backwards-scattered light in one device, as shown in Figs. 3 and 4. Accordingly, an optical access in one dimension is sufficient and

Fig. 2 Linearized calibration curve $q^*(y)$ and the associated fringe spacings $d_i(y)$
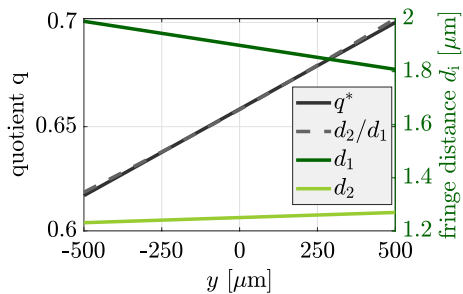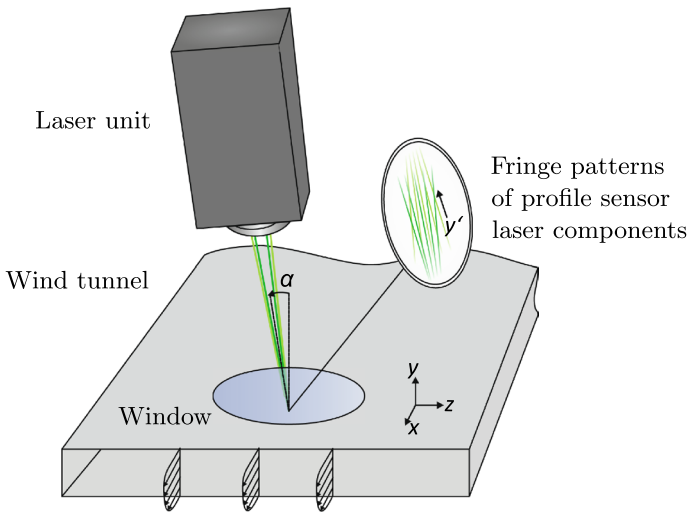
Fig. 3 Experimental Setup: LDV-PS on top of the wind tunnel, only the laser beam pairs of the LDV-PS are displayed. The detailed view shows convergently-divergently oriented interference fringes that form in the measurement volume in the $x-y$ plane
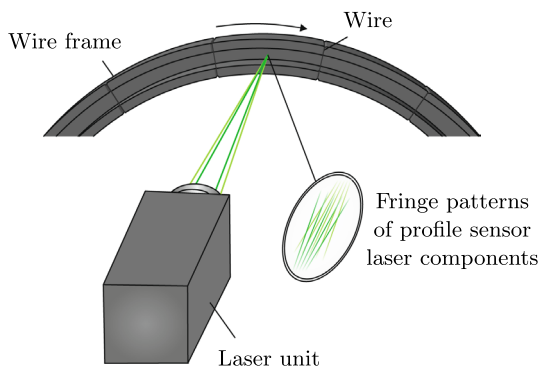

Fig. 4 Experimental Setup: LDV-PS facing the rotating wire frame, only the laser beam pairs of the LDV-PS are displayed. The detailed view shows convergently-divergently oriented interference fringes

the measurement unit can be traversed without the need to readjust individual components, making an extend FOV larger than the measurement volume length accessible at moderate effort. The measurement volume length is specified as about 500–3000 μm by the manufacturer depending for the focal length, i.e. 500–1000 μm for the here-used system. Note, that this, compared to LDV, large measurement volume is not identical to the spatial resolution for the LDV-PS.

2.2 Setup of the Turbulent Channel Flow Measurements

The turbulent flow measurements are conducted in a channel (duct) flow facility as already used by Hehner et al. (2021) and von Deyn et al. (2022) for active and passive flow control

investigations, respectively. The test-section has a cross section of 300 mm × 25.2 mm (width × height) corresponding aspect ratio of 12 and an overall length of 4000 mm to ensure that the turbulent flow achieves a fully developed state. The top wall of the test section is additionally equipped with a flush-mounted anti-reflection coated float glass window (1 mm thickness) to ensure a high quality, low distortion optical access to the measurement domain 100 mm upstream of the channel outlet as illustrated in Fig. 3. The experiments are performed at a Reynolds number of 7000 based on the centerline velocity of $U_{cl} = 8.4$ m/s and the channel half height. This corresponds to a friction Reynolds number of 350.

The wind tunnel is seeded with Di-Ethyl-Hexyl-Sebacate (DEHS) tracer particles of a nominal diameter of $d = 1\,\mu m$, and the measurement system and corresponding fringe patterns are oriented to measure the wall normal profile of the main velocity component, i.e. $u(y)$. To avoid reflection issues at the lower wall, the sensor is furthermore tilted by $\alpha = 20°$ around the x axis as shown in Fig. 3 and the measured position values y' are subsequently corrected by means of trigonometric relations to determine y. In the channel flow, the measurement volume is traversed in 500 μm steps to capture the velocity profile continuously in the lower channel half and the measurements are conducted through the transparent top wall in the lower half of the cross section.

The y-value measurement range per measurement volume location is limited to 2000 μm within each individual measurement to limit the increasing measurement uncertainty at increasing distance from the measurement volume center. The Fast-Fourier Transform (FFT) sampling frequency is chosen to 100 MHz with a sample number of 2048 for the velocity evaluation of the individual burst-event signals.

2.3 Setup of the Characterization Experiment

The characterization experiment is conducted on a modified existing test rig for clutch-flow investigations (see Leister et al. 2021, 2022, for rig details) equipped with a precise nanotec ST11018L8004 stepping motor. Wires of 5 μm, 10 μm, 13 μm, 20 μm, 40 μm and 80 μm diameter are attached radially along the perimeter of a 3D-printed circular frame, which is mounted on the test rig to ensure a constant and identical circumferential velocity $u_\phi = \Omega r$ for all wires at the investigated angular speeds Ω; see Fig. 4. Tungsten wires are used for the study, as these wires are available across a wide range of small diameters with a good geometrical accuracy of $\pm 10\%$ down to the size range of seeding particles. A light barrier sensor WL100L-F2231 enables the retro-active determination of the rotation angle to distinguish the measurement data of the individual wires and thus allocate the recorded Doppler bursts to the respective wire diameters. As the frame radius is large compared to the size of the measurement volume, the trajectory of the wires through the measurement volume is approximated as linear. The sensor faces the wire frame, and is operated at a 5 MHz Bragg shift and tilted towards the axis of rotation for reflection prevention.

The theoretically derived expressions for the quantities in Eqs. (2) and (3) imply an influence of the relative frequency uncertainty of a burst signal evaluation. Therefore, the sample rate and sample number of the FFT are varied systematically in coordination with four different angular velocities Ω as listed in Table 1 and illustrated in Fig. 5. FFT sample rate and sample number are defined as constant values for each individual measurement in the ILA R&D LDV-software. For the first investigated acquisition mode, the acquisition rate and number of samples used for the FFT is held constant as indicated in the upper part of Fig. 5. This acquisition mode is especially advantageous, when the velocities of the investigated flow field are unknown. Furthermore, the measurement effort is comparatively

Table 1 Acquisition settings of the individual measurements; reference case appears in **bold** font. The sample number was 2048 for all shown cases

Rotation freq. [Hz]	Velocity [m/s]	Sample rate [MHz]
1	0.55	50
		25
2	**1.1**	**50**
4	2.2	50
		100
8	4.4	50
		130*

*chosen value (below the desired $4 \times 50 = 200$ MHz) due to hardware limitation of the applied sensor

small as all data can be acquired straight forwardly with the same set of parameters in one individual run. Then, for the second acquisition mode, the sample number per burst is kept constant and the sample rate is adjusted accordingly to record the constant number of samples across the same period length of a burst independent of the wire velocities; see lower part of Fig. 5. It is worth to mention that for this latter acquisition case the settings have to be adjusted to the measured velocity level, which makes flow measurements of velocity gradients and turbulent fluctuations more complex.

3 Measurement Data Processing, Results and Discussion

The LDV-PS measurements are thoroughly described in the present section. In a first step, the recorded signals of the measurements in the turbulent channel flow are introduced and discussed in Sect. 3.1, where additional emphasis is placed on the chosen post-processing routines for the scattered data. This comparative discussion on appropriate post-processing strategies rises further, more measurement-scientific, questions, which are particularly addressed in Sect. 3.2. In a final step, on basis of the insights derived from the characterization study, the experimentally obtained channel flow data set is further evaluated in Sect. 3.3 by means of a comparison to reference direct numerical simulation (DNS) data.

3.1 Turbulent Channel Flow Measurement Data

Figure 6 shows a scatter plot of velocity and position of approximately 624 000 particle bursts that were detected in the lower channel half with the settings described in Sect. 2.2. The alternation of lighter and darker shades in the diagram refer to each of the measurement series obtained at different traverse positions of the sensor, and thus of the measurement volume. The black asterisk indicates the channel half-height position and velocity, estimated as the maximum velocity from averaged measured velocity values in y-position bins in the central channel region. At small flow velocities, an increased scatter of measured values can be observed. The scattering of position values is limited to the maximum measurement range of 2000 μm, corresponding to approximately four times the measurement volume length. A small amount of approximately 500 bursts is registered with small negative velocities up to 0.03 m/s, which are expected in the viscous sublayer (Lenaers et al. 2012).
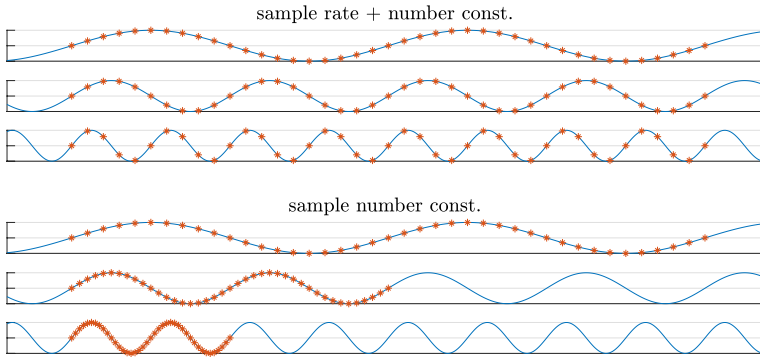
Fig. 5 Investigated acquisition modes of the characterization experiment. Upper part: sample rate and sample number remain constant for all investigated velocities; lower part: sample number remains constant, sample rate is adjusted to maintain identical sample numbers per burst for all investigated velocities
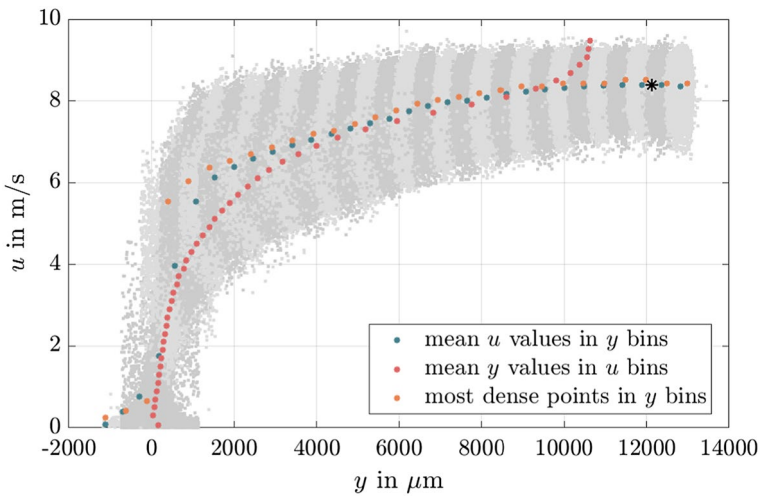

Fig. 6 Velocity and position values of the bursts registered in the turbulent channel flow ●● and different data averaging approaches (●)(●)(●)

In order to achieve mean velocity profiles $U(y)$ from the recorded scattered data, different post-processing routines have been suggested for LDV-PS measurements in the literature. Shirai et al. (2006) used the averaged position and velocity of 200 neighboring particle bursts, while Neumann et al. (2013) applied a so-called slotting technique to reveal spatially down-sampled gridded data from the LDV-PS raw data. This slotting has been applied by Burgmann et al. (2021), who averaged the velocity values of bursts within the same 10 μm-range of detected y-positions. In an attempt to advance beyond the prescribed limits of the evaluated bins, Strauch et al. (2022) proposed a post-processing routine based on the evaluation of most dense points in the velocity profile data. The maximum of the density distribution of measured velocity and position values was then evaluated within position bins.
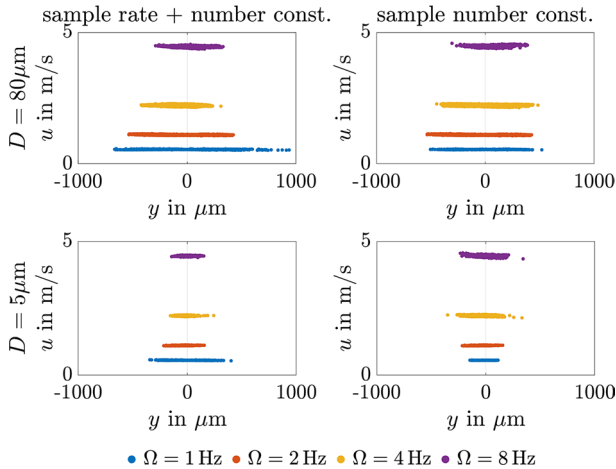
Fig. 7 Distributions of detected wire velocities and corresponding positions for different velocity levels, wire diameters D and acquisition modes

The results of the latter two approaches are shown superimposed to the raw data in Fig. 6, where the averaged velocity values across 470 μm-wide y bins (•) and most dense points together with averaged position values corresponding to 0.2 m/s-wide velocity bins (•). In an additional approach tested by Fuchs et al. (2023) the respective average y locations within velocity bins are analyzed, which is additionally shown for the present measurement data in Fig. 6(•). This latter method serves as a straight-forward evaluation approach to interpret the recorded LDV-PS data close to the wall, where steep velocity gradients occur and, moreover, the increasing scatter margin of measurement values makes the determination of the wall position challenging. Accordingly, the absolute position values shown in Fig. 6 build upon the wall position found with a linear fit of mean position values in 0.2 m/s wide velocity bins at flow velocities up to 2 m/s.

Consequently, the comparison of the three different post-processing strategies indicates that the mean velocity profile as well as the correspondingly expected wall position depend on the applied processing routine. As the observed distribution of detected bursts represents a superposition of the mean velocity profile, turbulent fluctuations and measurement uncertainty, the differentiation of these quantities is required for the development of a suitable data-processing routine. Considering the underlying determination procedure of a passing tracer-particle's velocity and position of the LDV-PS described in Sect. 2.1, it becomes clear that also the measurement accuracy of both quantities are mutually linked to each other. In order to investigate the effects of the internal signal-processing evaluation together with the arising position and velocity-measurement accuracy a characterization study is conducted, where both position and velocity measurements can be investigated separately. Subsequently, on basis of the results achieved for a set of systematically varied parameters the measurement data can be further evaluated as described below.

3.2 Evaluation of the Characterization Experiment

As introduced above, the extended parametric characterization experiment investigates the interplay between the size of the scattering object, a broad range of chosen LDV-PS

acquisition parameters, the velocity range within the observed measurement volume, and the accuracy of the velocity and position estimation. The conducted measurements comprise two acquisition modes, four velocities (see Table 1 and Fig. 5 for details and illustration) and six wire diameters.

The distributions of detected wire velocities and correspondingly determined wire positions are shown in Fig. 7 for the 5 μm- and 80 μm-diameter wires (top and bottom row, respectively). As to be expected, σ_y decreases for thinner wires for both acquisition cases. The relative velocity standard deviation σ_u/u is in the range of 0.4 % – 0.6 % for all wires and cases with slightly increasing relative velocity standard deviations for larger wire diameters. The scatter distribution of the obtained y-position values resembles a Gaussian distribution.

For the first acquisition case with constant sample rate and number in the scattered light signal processing FFT (left column of Fig. 7), the spatial uncertainty increases with decreasing velocities. This effect has been observed also in the turbulent channel flow and can be explained by the different burst-signal representations of the evaluated samples. While the temporal window size remains constant, the duration and corresponding period length of the Doppler bursts increases with decreasing velocity, which is indicated in Fig. 8. Consequently, the excluded margin of the registered bursts increases for lower velocities so that an accordingly smaller proportion of the burst signal is evaluated at likewise diminished relative sample rate.

This truncation of the burst signal inevitably leads to a lack of information and is, therefore, expected to cause the observed measurement uncertainty to increase at low velocities. To overcome this velocity-related shortcoming, the second acquisition mode, in contrast, adapts the sample rate to the expected velocity magnitude, which accordingly renders the position-estimation uncertainty to become independent from the considered velocity level. The wire results for this acquisition mode of constant (relative) period resolution and period length of a burst signal for all considered wire velocities are shown in the right column of Fig. 7, which indeed indicate the expected constant accuracy for this LDV-PS operation mode.

Furthermore, as shown in Eq. (2), the position measurement accuracy σ_y additionally depends on the quotient-function slope $\partial y/\partial q$ and the quotient-function accuracy σ_f (see also Czarske et al. 2002). For the used LDV-PS measurement system, this quotient function is approximated by a linear function as illustrated in Fig. 2, which causes an increasing measurement error with increasing distance from the measurement volume center at $y = 0$ (cf. q^* and d_2/d_1). The slope $\partial y/\partial q$ of the used measurement system is 12 041 μm, whereas a slope of 7 143 μm was reported for a different LDV-PS set-up by Shirai et al. (2006), where the latter weaker value accordingly leads to an approximately halved calculated z-position standard deviation. This difference in the slope of the quotient function occurs due to a larger focal length of the employed commercial LDV-PS system.

An evaluation of the particle-diameter influence on the resulting position measurement accuracy σ_y is shown in Fig. 9, which compares the linear regression curves of the y-position standard deviations σ_y for all investigated wire diameters D, all four angular velocities Ω and both acquisition modes. As indicated in the left diagram, in case of acquisition at constant sample rate and number the aforementioned velocity-dependent uncertainty leads to a quasi-constant shift of the curves, which accordingly appear sorted by the respective wire velocity, i.e. increasing standard deviation for decreasing velocities. This clear velocity-related separation is not observed for an acquisition with velocity-adjusted sample rate (right diagram of Fig. 9), where the curves of all investigated angular velocities collapse. The slope dy/dD of the curves varies in the range from 0.67 to 1.21 with an average slope

of 0.91 for both considered acquisition modes. Since this average value is approximately 1, it is consequently hypothesized that the y-position standard deviation immediately scales with the chosen tracer-particle diameter, which is mimicked by the wires in the present study. It is likewise expected that σ_y is limited to the particle diameter as a minimum, since light is scattered at the particle surface when passing the measurement volume.

It is important to note, that the observed standard deviations are additionally influenced by individual and global sources of uncertainty related to the chosen experimental setup. In the present context, these include the wire-diameter uncertainty, the hand-mounting process of the wires, vibrations of the test rig, thermo-mechanical effects on the wires caused by the laser radiation and possibly velocity dependent dynamic behaviour of the wires. Most of these factors can not be determined quantitatively for the conducted experiments, but may explain the observed scatter margin of the measurement data of individual wires in Fig. 9. A quantitative evaluation of test-rig vibration-caused y-position fluctuations has been measured by means of a triangulation sensor for $\Omega = 1\,\text{Hz}$, $2\,\text{Hz}$ and is found to range between 10 μm and 20 μm. Accordingly, a vertical downward shift of the standard deviation curves shown in Fig. 9 corresponds to the measurement uncertainty of the system without the influence of the vibrations.

3.3 Evaluation of the Turbulent Channel Flow Measurements

The LDV-PS measurement data can now be evaluated based on the findings of the characterization study. The y-position uncertainty is found to be limited to the size of the tracer particles in the characterization experiment, which is in the order of magnitude of 1 μm for DEHS particles in the conducted measurement and, thus, small compared to the measurement uncertainty induced by the signal processing at decreasing velocities (cf. left diagram of Fig. 9). The vibrations of the lower channel flow were measured by means of a triangulation sensor and did not exceed 1 μm. Furthermore, the study reveals an increasing position measurement uncertainty at decreasing velocities for constant FFT parameters, which is observed at low flow velocities (cf. Fig. 6). As such, the scattering of measurement data in the near wall region of the turbulent channel flow represents a position measurement uncertainty rather than a characteristic of the flow.

To further examine this effect, the registered particle velocity and position distribution is shown in Fig. 10, where lighter shades indicate a lower and darker shades a higher burst density. The number of detected burst events is determined in 0.2 m/s wide velocity bins
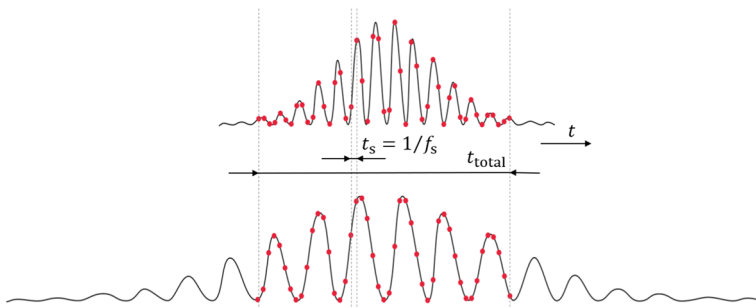

Fig. 8 Sketch of two Doppler bursts at different particle velocities and the relative distribution of a constant sample number and rate within either burst
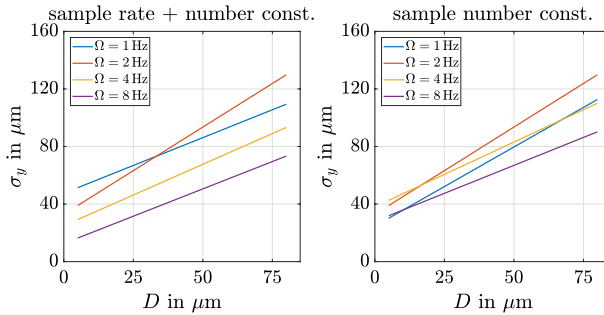
Fig. 9 Fitted linear curves for *y*-position standard deviation over wire diameter *D* for all four velocity levels of both acquisition modes

and 200 μm wide position bins, and is afterwards normalized by the maximum number of bursts found at all velocity bins within the same position bin.

In order to allow an immediate interpretation of the shown data, the normalized probability density distribution of the flow velocity over channel wall distance for DNS data at $Re_\tau = 590$ (Alfredsson et al. 2011) is superimposed to the diagram as black solid lines. The DNS results were, therefore, converted to physical units assuming the facility channel height and air viscosity to allow for immediate data comparison. This was preferred instead of converting the measured data into inner-scaled quantities due to the different mean-velocity gradients depending on the averaging methods for the LDV-PS.

A good agreement of the probability density distribution of the measurements and the DNS data is found for position values $y > 2000$ μm, while closer to the wall the measurement uncertainty increases due to the factors elaborated in Sect. 3.2. Particularly for the range $y < 1000$ μm this deviation reveals a significantly larger scatter margin of the LDV-PS data due to the increasing position-estimation uncertainty for the lowest velocity range above the wall. While the velocity-fluctuation amplitude is large in this region as shown by the DNS reference data, a decrease to zero is by definition expected at the wall. In fact, the streamwise velocity PDF is known to be log-normal and therefore strongly asymmetric (Alfredsson et al. 2011) as can also be inferred from the DNS contour lines. The reason why the LDV-PS data exhibits a near Gaussian distribution with nonphysical values is related to the inherent background noise level as also known from LDV measurements, which shows up when the absolute fluctuation level goes below the noise floor. Additionally, as the scattering of position values is found to be approximately Gaussian distributed in the characterization study, it becomes clear that a mean velocity profile based on *y*-bin averaging, represented by the blue circles, in fact is no suitable representation of the flow physics in the vicinity of the wall for the present measurement data.

It must be noted that the underlying approximation of the wall position from the LDV-PS measurement data as well as the relative traverse positions remain a source of uncertainty in these considerations. The so-called diagnostic plot (Alfredsson et al. 2021) allows the comparison of turbulent shear flow data without the need to determine the wall position nor the friction velocity. Figure 11 shows such a diagnostic plot for the present investigation, where the ratio of the rms level of streamwise velocity to mean streamwise velocity u_{rms}/U is plotted over the ratio of mean streamwise velocity to centerline velocity U/U_{cl}. Recall from above, that – similar to the mean quantities – also the *u*-rms values can only be evaluated within data bins, which in the present case has been the *y*-position binning as already applied for the blue data points of the mean velocity profile in Fig. 6.
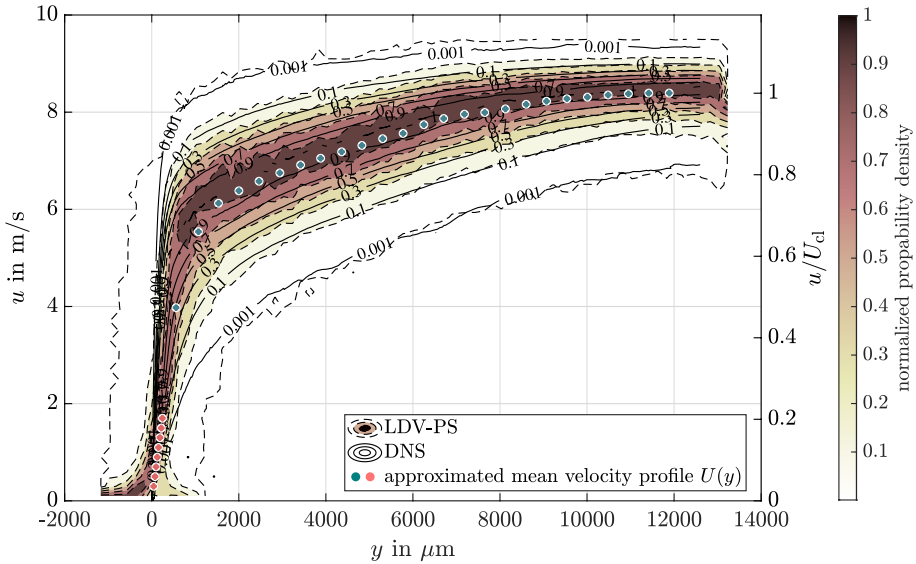
Fig. 10 Comparison of normalized probability density distribution of the measurement results and reference DNS data at $Re_\tau = 590$ (Alfredsson et al. 2011). The number of bursts within 0.2 m/s wide velocity bins and 470 μm wide position bins normalized with the maximum number of bursts at the same position. The approximated mean velocity profile based on u-bin averaged velocity values close to the wall (●) and y bin averaged position values in the channel centre region (●) is indicated with the circles

A good agreement is found with DNS reference data by Moser et al. (1999) at $Re_\tau = 390$ and 590 for mean flow velocities $U > 0.7U_{cl}$, which confirms the quality of the determined mean and rms velocity values for the outer region, i.e. at approximately $y > 0.15\delta$ (Alfredsson and Örlü 2010). To allow further comparison of tracer-based velocimetry approaches for the given flow scenario, the stereo PIV results of Hehner et al. (2021) are also added to the diagnostic plot. Interestingly, the PIV data remain on the DNS curve towards lower relative velocities u/U_{cl} as compared to the LDV-PS approach. This immediate comparison of the experimental results indicates that measurement-uncertainty related contributions to the u_{rms} level of the experimental data adversely affects the LDV-PS procedure up to larger velocities – thus wall distances – as compared to the PIV approach.

Finally, we aim to extract the mean velocity profile in inner scaling from the LDV-PS data and compare it to velocity data from DNS. In order to convert the present data into dimensionless viscous + units, different approaches are presented and discussed. Here, the superscript + indicates nondimensionalisation by the kinematic viscosity ν of the fluid and the friction velocity $u_\tau = \sqrt{\tau_w/\rho}$, where τ_w denotes the mean wall shear stress and ρ the fluid density. Firstly, as described by Hehner et al. (2021), the present data can be fitted to a composite velocity profile description such as the one by Luchini (2018) in order to find the corresponding friction Reynolds number Re_τ and wall position simultaneously. Alternatively, the wall shear stress τ_w can be determined directly from the mean velocity gradient in the viscous sublayer, if it is measured with sufficient measurement accuracy and spatial resolution. Note that we abstain from using the wall-shear stress from the (global) pressure-drop measurements, since the reason for testing the LDV-PS in turbulent channel flow is the access of local wall shear stress information.

Fig. 11 Diagnostic plot of LDV-PS measurement data evaluated in 470 µm wide y-position bins together with reference DNS data at $Re_\tau = 390$ an 590 (Moser et al. 1999) and stereo PIV data at $Re_\tau = 358$ (Hehner et al. 2021)
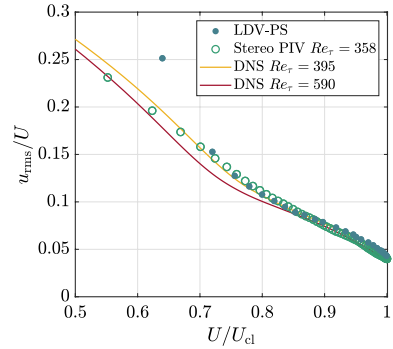

Fig. 12 Mean velocity profile evaluated in 0.2 m/s wide velocity bins(•) and 470 µm wide y-position bins(•) of LDV-PS measurements compared with DNS data at $Re_\tau = 390$ (Moser et al. 1999) and stereo PIV data at $Re_\tau = 358$ (Hehner et al. 2021). The physical coordinates on the upper and right axes refer to the profile sensor measurements at $Re_\tau = 350$. All registered velocity and position values are shown in the background (•)
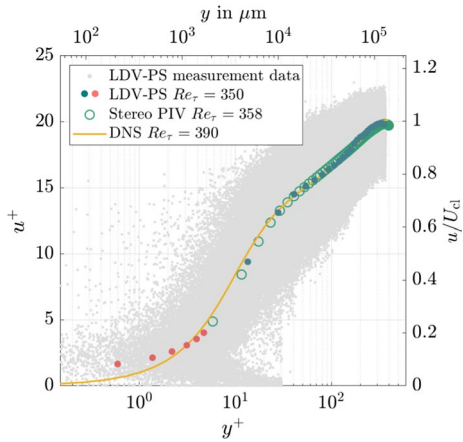
A mean velocity profile based on a combination of u-bin averaging in the near wall region (•) and y-bin averaging in the channel center region (•) is considered, which is respectively indicated by the red and blue circles in Fig. 10 in consistency with the color-coding of Fig. 6. The evaluation of most dense points suggested by Strauch et al. (2022) shown in Fig. 6 is observed to overshoot the average-based mean velocity profile, which is likely to be related to the effect that more particles cross the LDV measurement volume at higher velocities (Albrecht et al. 2013). The y-bin averaging is therefore expected to be less biased by this effect and accordingly to be a better representation of the flow. Additionally, correction procedures for mean velocities measured with LDV have been presented in literature (Albrecht et al. 2013).

Based on this combined velocity profile, first Re_τ and the wall position are estimated simultaneously by means of a least-square fit function using the general description of the dimensionless mean velocity profile by Luchini (2018). Figure 12 shows the mean velocity profile, where the lower abscissa axis and left ordinate axis show inner (viscous) scaling, while the upper abscissa axis and right ordinate axis present physical coordinates to also maintain direct comparability with Fig. 10 and 11. Additionally, DNS data from Moser et al. (1999) at $Re_\tau = 390$ and stereo PIV measurements from Hehner et al. (2021) at $Re_\tau = 358$ are shown for reference and comparison purposes, respectively. The velocity and position values of all registered bursts are shown in the background (•).

The mean velocity profile overall agrees with the reference profiles. Nevertheless, deviations occur in the near-wall region. Accordingly, the determination of the viscous scales based on the evaluation of the wall shear stress using the velocity gradient in the wall near region of the viscous sublayer leads to an underestimation of the friction Reynolds number and, thus, does not lead to an appropriate scaling for the largest portion of the profile, even though a sufficient amount of particle bursts was detected in the region of the viscous sublayer. For the stereo PIV measurements, in comparison, the first measurement point is at $y^+ = 6$ for a similar Re_τ. The deviation of the LDV-PS velocity profile from the references in the wall near region is represented by overshooting velocity values close to the wall. This effect might be associated with decreasing particle density towards the wall and the occurrence of the LDV-typical bias to detect more particles at higher velocities (Albrecht et al. 2013), which is especially pronounced at high velocity gradients. Based on such a shifted particle density distribution, the mean position values are underestimated within velocity bins, as can be observed in Fig. 12.

The comparison of the mean velocity profile of the flow emphasizes the findings revealed in the diagnostic plot. Good agreement of the measured mean and rms velocity profiles with reference data is shown at larger mean velocities towards the channel center, where the measurement system related uncertainty is small. Though, since the effect of slightly overshooting mean velocity values is less pronounced in the diagnostic plot (cf. Fig. 11), the measured rms values in the centre region are found to be slightly overestimated as well. Overall, Fig. 10 confirms the accordance of the probability density distribution of the measurement data with DNS data over the entire outer region of the channel flow. In the direct proximity of the wall, in contrast, the increasing position-determination uncertainty at low velocity levels together with the large velocity gradient lead to large deviations of the rms and probability density distribution values from the reference data. As such, the distinction of turbulent velocity fluctuations and measurement uncertainty remains a challenge for LDV-PS measurements in unknown flows. None of the suggested processing approaches allowed the direct measurement of the wall shear stress from the shown measurement data.

4 Conclusions and Outlook

The employed LDV-PS measurement system was found to provide spatially and temporally resolved velocity data in the outer region of the turbulent channel flow based on the statistical evaluation of the measurement data shown in Fig. 11. As such, it is a beneficial tool for flow measurements especially in facilities with limited accessibility for intrusive probes or multiple optical components. The evaluation of the measurement data gathered in the inner region and a separate characterization experiment showed an increasing measurement uncertainty at decreasing velocity levels, thus indicating limited suitability of the measurement system in low-velocity flow measurements. Particle bursts could be detected over the whole channel height with the chosen setup, proving that the region of the viscous sublayer is in principle accessible with the measurement system. The observed velocity-dependent scatter margin of the location estimation has been identified to be dominated by the internal signal processing of the scattered light signal of the measurement system. It has to be concluded accordingly, that a flow-velocity dependent choice of FFT parameters is required to achieve constant (low) measurement uncertainty, allowing the evaluation of turbulent statistics at small local flow velocities.

Additionally, possible sources of measurement inaccuracy arise from the dynamic behaviour of the test setup during the experiments as well as the scattering object size, as evidenced by the increase of the wire diameter in the characterization experiment, which caused an increase of the measurement uncertainty of approximately the same value. The latter factor might complicate measurements in liquid with overall larger particles.

The determination of turbulence statistics is directly influenced by the particle density distribution of measured velocity and position values, which depends on the choice of traversing steps and respective measurement durations. A continuous, homogeneous burst distribution, therefore, requires fine traversing of the LDV-PS in the order of magnitude of the measurement volume length and increased measurement times at high velocity gradients, which might be accompanied by an increased measurement effort. Additionally, the reduced amount of particles near the wall and a potentially decreasing signal-to-noise ratio due to light scattered at the wall need to be considered in the interpretation of data. The possibility of limiting the position measurement range in the LDV-PS software can reduce the position scattering of a measurement. Though, this might make the statistical processing of the data more difficult, as the scattering of detected particles is not captured as a whole anymore. Furthermore, general LDV-specific bias errors occur due to the measurement volume shape with regard to the velocity-profile slope as well as the higher number of faster particles passing the measurement volume, which could be corrected based on the individual particle passing time.

It was shown that different data evaluation approaches used in the literature led to varying results for the introduced measurement data, which demonstrates the need for consistent and comprehensible documentation. As a final remark towards future LDV-PS-based flow investigations, a transparent, uniform and robust data processing routine seems mandatory, to ensure an objective analysis of flow statistics and measurement uncertainties.

The work summarized in this manuscript was initiated to document the capability of the commercially available LDV-PS to measure a turbulent channel flow and corresponding near-wall turbulence statistics. However, as described above, this step indicates that further work is needed to be able to use the LDV-PS as a reliable off-the-shelf technique for measurements in flows with large velocity gradients. Especially after performing comprehensive analyses of the observed measurement characteristics, this otherwise preliminary verification step is considered important knowledge to share with the scientific community.

Author Contributions SP Conceptualization, Methodology, Formal Analysis, Investigation, Data curation, Visualization, Writing - original draft; RL Conceptualization, Methodology, Formal Analysis, Writing - review & editing; DG Formal Analysis, Supervision, Writing - review & editing; RÖ Formal Analysis, Writing - review & editing; BF Resources, Writing - review & editing; JK Conceptualization, Methodology, Supervision, Writing - review & editing.

Declarations

Conflict of interest The authors declare that they have no conflict of interest.

References

Albrecht, H.E., Damaschke, N., Borys, M., et al.: Laser Doppler and phase Doppler measurement techniques. Springer Sci. Bus. Med. (2013). https://doi.org/10.1007/978-3-662-05165-8_2

Alfredsson, P.H., Örlü, R.: The diagnostic plot-a litmus test for wall bounded turbulence data. Eur. J. Mech. B/Fluids **29**(6), 403–406 (2010). https://doi.org/10.1016/j.euromechflu.2010.07.006

Alfredsson, P.H., Örlü, R., Schlatter, P.: The viscous sublayer revisited-exploiting self-similarity to determine the wall position and friction velocity. Exp. Fluids **51**(1), 271–280 (2011). https://doi.org/10.1007/s00348-011-1048-8

Alfredsson, P.H., Segalini, A., Örlü, R.: The diagnostic plot-a tutorial with a ten year perspective. In: Progress in Turbulence IX: Proceedings of the iTi Conference on Turbulence 2021, Springer, pp. 125–135, (2021) https://doi.org/10.1007/978-3-030-80716-0_17

Bayer, C., Shirai, K., Büttner, L., et al.: Measurement of acceleration and multiple velocity components using a laser Doppler velocity profile sensor. Measurement Sci. Technol. **19**(5), 055401 (2008)

Benard, N., Moreau, E.: Electrical and mechanical characteristics of surface ac dielectric barrier discharge plasma actuators applied to airflow control. Exp. Fluids **55**(11), 1846 (2014). https://doi.org/10.1007/s00348-014-1846-x

Bürkle, F., Moyon, F., Feierabend, L., et al.: Investigation and Equalisation of the flow distribution in a fuel cell stack. J. Power Sources (2020). https://doi.org/10.1016/j.jpowsour.2019.227546

Bürkle, F., Czarske, J., Büttner, L.: Simultaneous velocity profile and temperature profile measurements in microfluidics. Flow Measurement Instrum. (2022). https://doi.org/10.1016/j.flowmeasinst.2021.102106

Bürkle, F., Förste, M., Dadzis, K., et al.: Application of optical velocity measurements including a novel calibration technique for micron-resolution to investigate the gas flow in a model experiment for crystal growth. Flow Measurement Instrum. (2022). https://doi.org/10.1016/j.flowmeasinst.2022.102258

Bruun, H.H.: Hot-wire anemometry: principles and signal analysis (1995)

Burgmann, S., Dues, M., Barwari, B., et al.: Flow measurements in the wake of an adhering and oscillating droplet using laser-doppler velocity profile sensor. Exp. Fluids **62**(3), 1–16 (2021). https://doi.org/10.1007/s00348-021-03148-0

Büttner, L., Czarske, J.: Spatial resolving laser Doppler velocity profile sensor using slightly tilted fringe systems and phase evaluation. Meas. Sci. Technol. **14**(12), 2111 (2003). https://doi.org/10.1088/0957-0233/14/12/010

Büttner, L., Czarske, J.: Determination of the axial velocity component by a laser-Doppler velocity profile sensor. J. Opt. Soc. Am. A **23**(2), 444–454 (2006). https://doi.org/10.1364/josaa.23.000444

Cierpka, C., Scharnowski, S., Kähler, C.J.: Parallax correction for precise near-wall flow investigations using particle imaging. Appl. Opt. **52**(12), 2923–2931 (2013). https://doi.org/10.1364/AO.52.002923

Czarske, J.: Laser Doppler velocity profile sensor using a chromatic coding. Meas. Sci. Technol. **12**(1), 52 (2001). https://doi.org/10.1088/0957-0233/12/1/306

Czarske, J., Büttner, L., Razik, T., et al.: Boundary layer velocity measurements by a laser Doppler profile sensor with micrometre spatial resolution. Meas. Sci. Technol. **13**(12), 1979 (2002). https://doi.org/10.1088/0957-0233/13/12/324

von Deyn, L.H., Schmidt, M., Örlü, R., et al.: Ridge-type roughness: from turbulent channel flow to internal combustion engine. Exp. Fluids **63**(1), 18 (2022). https://doi.org/10.1007/s00348-021-03353-x

Fan, Y., Arwatz, G., Van Buren, T., et al.: Nanoscale sensing devices for turbulence measurements. Exp. Fluids **56**, 138 (2015). https://doi.org/10.1007/s00348-015-2000-0

Fuchs, T., Bross, M., Kähler, C.J.: Wall-shear-stress measurements using volumetric μPTV. Exp. Fluids (2023). https://doi.org/10.1007/s00348-023-03656-1

Haufe, D., Pietzonka, S., Schulz, A., et al.: Aeroacoustic near-field measurements with microscale resolution. Measurement Sci. Technol. **25**(10), 105301 (2014). https://doi.org/10.1088/0957-0233/25/10/105301

Hehner, M.T., von Deyn, L.H., Serpieri, J., et al.: Stereo PIV measurements of oscillatory plasma forcing in the cross-plane of a channel flow. In: 14th International Symposium on Particle Image Velocimetry, (2021). https://doi.org/10.18409/ispiv.v1i1.117

ILA R&D GmbH (2023) Commerical LDV-PS product website. https://ila-rnd.com/ldv-profile-sensor/

Kähler, C.J., Scharnowski, S., Cierpka, C.: On the uncertainty of digital PIV and PTV near walls. Exp. Fluids **52**(6), 1641–1656 (2012). https://doi.org/10.1007/s00348-012-1307-3

Kotsonis, M.: Diagnostics for characterisation of plasma actuators. Measurement Sci. Technol. **26**(9), 092001 (2015). https://doi.org/10.1088/0957-0233/26/9/092001

Leister, R., Fuchs, T., Mattern, P., et al.: Flow-structure identification in a radially grooved open wet clutch by means of defocusing particle tracking velocimetry. Exp. Fluids **62**(2), 1–14 (2021). https://doi.org/10.1007/s00348-020-03116-0

Leister, R., Pasch, S., Kriegseis, J.: On the applicability of LDV profile-sensors for periodic open wet clutch flow scenarios. Exp. Fluids **63**(8), 134 (2022). https://doi.org/10.1007/s00348-022-03487-6

Lenaers, P., Li, Q., Brethouwer, G., et al.: Rare backflow and extreme wall-normal velocity fluctuations in near-wall turbulence. Physics of Fluids **24**(3), 035110 (2012). https://doi.org/10.1063/1.3696304

Ligrani, P., Bradshaw, P.: Subminiature hot-wire sensors: development and use. J. Phys. E Sci. Instrum. **20**(3), 323 (1987). https://doi.org/10.1088/0022-3735/20/3/019

Luchini, P.: Structure and interpolation of the turbulent velocity profile in parallel flow. Eur. J. Mech. B/Fluids **71**, 15–34 (2018). https://doi.org/10.1016/j.euromechflu.2018.03.006

Meinhart, C., Wereley, S., Santiago, J.: Micron-resolution velocimetry techniques. In: Laser Techniques Applied to Fluid Mechanics: Selected Papers from the 9th International Symposium Lisbon, Portugal, July 13–16, 1998. Springer Science & Business Media, pp. 57–70 (2000), https://doi.org/10.1007/978-3-642-56963-0_4

Moser, R.D., Kim, J., Mansour, N.N.: Direct numerical simulation of turbulent channel flow up to $Re_\tau = 590$. Phys. Fluids **11**(4), 943–945 (1999). https://doi.org/10.1063/1.869966

Neumann, M., Friedrich, C., Czarske, J., et al.: Determination of the phase-resolved body force produced by a dielectric barrier discharge plasma actuator. J. Phys. D Appl. Phys. **46**(4), 042001 (2013). https://doi.org/10.1088/0022-3727/46/4/042001

Örlü, R., Vinuesa, R.: Instantaneous wall-shear-stress measurements: advances and application to near-wall extreme events. Measur. Sci. Technol. **31**(11), 112001 (2020). https://doi.org/10.1088/1361-6501/aba06f

Pasch, S., Leister, R., Egner, M., et al.: Comparative accuracy study of LDV profile-sensor acquisition modes and particle diameters. In: 20th International Symposium on the Application of Laser and Imaging Techniques to Fluid Mechanics, Lisbon, Portugal, (2022). https://doi.org/10.5445/IR/1000157961

Raffel, M., Willert, C.E., Scarano, F., et al.: Particle image velocimetry: a practical guide, 3rd edn. Springer Cham, (2018). https://doi.org/10.1007/978-3-319-68852-7

Shirai, K., Pfister, T., Büttner, L., et al.: Highly spatially resolved velocity measurements of a turbulent channel flow by a fiber-optic heterodyne laser-Doppler velocity-profile sensor. Exp. Fluids **40**(3), 473–481 (2006). https://doi.org/10.1007/s00348-005-0088-3

Strauch, C., Peter, J., Dues, M., et al.: Application of LDV profile sensor technology for velocity determination in small axial gaps. In: 20th International Symposium on the Application of Laser and Imaging Techniques to Fluid Mechanics, Lisbon, Portugal (2022)

Tropea, C., Yarin, A.L., Foss, J.F., et al.: Springer handbook of experimental fluid mechanics. Springer (2007). https://doi.org/10.1007/978-3-540-30299-5